

# Effect of Metal Oxides on Reaction Route and Product Distribution of Catalytic Cellulose Hydrogenolysis

Guifang Fan,<sup>a,b,\*</sup> De Chen,<sup>c</sup> Shizhong Li,<sup>a,b</sup> Mingde Yang,<sup>a</sup> and Yulong Wu<sup>a</sup>

The effects of CeO<sub>2</sub>, ZrO<sub>2</sub>, Nb<sub>2</sub>O<sub>5</sub>, and ZnO catalysts supported on carbon nanotubes (CNT) relative to cellulose hydrothermal hydrogenolysis in the presence of Ni/CNT and pressured H<sub>2</sub> was studied in this work. The catalysts were characterized by inductively coupled plasma – optical emission spectrometry, X-ray diffraction, X-ray photoelectron spectrometry, transmission electron microscopy, NH<sub>3</sub> temperature programmed desorption (TPD), and CO<sub>2</sub>-TPD. Glucose and its isomers were detected by mass spectrometry. The results showed that redox active CeO<sub>2</sub>/CNT with strong Lewis acid and strong Lewis base sites was active in C-C bond cracking, isomerization, dehydrogenation, and hydrodeoxygenation reaction, yielding 36.3% ethylene glycol and 17.2% 1,2-propylene glycol. The ZnO/CNT with Bronsted base accelerated isomerization, retro-aldol condensation, and dehydrogenation, yielding 20.7% 1,2-propylene glycol, 17.8% ethylene glycol, and 12.7% tetrahydrofuran dimethanol. The Nb<sub>2</sub>O<sub>5</sub>/CNT and ZrO<sub>2</sub>/CNT were inert to C-C bond cracking, whereas H<sup>+</sup> in hot compressed water and the Bronsted acid in Nb<sub>2</sub>O<sub>5</sub>/CNT accelerated dehydration, yielding more sorbitol and sorbitans. The results provide reference for catalyst selection and product regulation in cellulose hydrogenolysis.

DOI: 10.15376/biores.18.4.7367-7390

Keywords: Cellulose hydrogenolysis; CeO<sub>2</sub>; ZnO; ZrO<sub>2</sub>; Nb<sub>2</sub>O<sub>5</sub>

Contact information: a: Institute of Nuclear and New Energy Technology, Tsinghua University, Beijing, 100084, China; b: Beijing Engineering Research Center of Biofuels, Tsinghua University, Beijing, 100084, China; c: Department of Chemical Engineering, Norwegian University of Science and Technology (NTNU) N-7491 Trondheim, Norway; \*Corresponding author: fanguifang@tsinghua.edu.cn

## INTRODUCTION

Biomass conversion, if carried out appropriately, offers the attractive feature of carbon neutrality. Catalytic degradation of cellulose to chemicals has attracted much attention in recent years. Hydrogenation can transform generated glucose to more stable compounds such as sorbitol, prevent the formation of humin (Maruani *et al.* 2018), and then increase the yields of products. Cellulose could be selectively converted to sorbitol, ethylene glycol (EG), and 1,2-propylene glycol (1,2-PG) by catalytic hydrogenation reactions (Sun *et al.* 2016; Lazaridis *et al.* 2017; Li *et al.* 2017; Gu *et al.* 2019; Li *et al.* 2019; Zan *et al.* 2019; Zhang *et al.* 2019; Zheng *et al.* 2017). By far, the highest yields of sorbitol, EG, and 1,2-PG are reported as 91% (Shrotri *et al.* 2018), 77.5% (Li *et al.* 2018), and 39% (Xiao *et al.* 2013), respectively. Sorbitol has been identified as one of the twelve most important building blocks derived from biomass resources, EG and 1,2-PG are raw materials for polymer industry. Cellulose catalytic hydrogenation into chemicals is an attractive alternative in its valorisation.

The catalytic hydrogenation of cellulose mainly includes the following steps: (1) cellulose hydrolyzed to glucose in the presence of H<sup>+</sup>, (2) glucose hydrogenated to sorbitol

with the catalysis of Ni, or noble metal atom, (3) sorbitol dehydrogenated back to hexose, or dehydration to sorbitan, (4) glucose isomerized to fructose in the presence of base or Lewis acid (Delidovich and Palkovits 2016; Nguyen *et al.* 2016), (5) glucose and fructose experienced Retro-Aldol Condensation (RAC), C-C breaking took place, formed lower aldose and ketose such as erythrose, glycolaldehyde, glyceraldehyde, 1,3-dihydroxyacetone, *etc.* (6) The products of RAC have been hydrogenated and dehydrated to EG, 1,2-PG, *etc.*

Isomerization and RAC are accelerated by base catalyst; however, homogeneous alkali catalysis will neutralize with  $H^+$  and hinder cellulose hydrolysis (Li *et al.* 2015). Metal oxides possess Lewis acid and basic sites, which catalyze isomerization and RAC reaction with no discount of cellulose conversion. The acid-base property of sparingly soluble oxides in contact with aqueous solutions are chiefly determined by the isoelectric point of solid surface (IEPS). For some metal oxides, the IEPS values are rather constant. The IEPS values of  $CeO_2$ ,  $ZnO$ ,  $ZrO_2$ , and  $Nb_2O_5$  were reported as being 8.1, 9.2, 7.8, and 4.1 (Kosmulski 1997). These findings mean that suspension of  $ZnO$  and  $Nb_2O_5$  are Brønsted base and acid, respectively.  $CeO_2$  is known as an oxygen storage substance (Montini *et al.* 2016).  $ZrO_2$  is a compound rich in Lewis acid and base sites (Huang *et al.* 2019). Carbonaceous materials are hydrothermal stable even at elevated temperatures (Pham *et al.* 2015). Carbon nanotubes and surface functionalized biochar were found to work well as catalyst support on hydrothermal conversion of biomass (Chen *et al.* 2017; Liu and Liu 2020). The effects of typical metal oxides catalysts such as  $CeO_2/CNT$ ,  $ZnO/CNT$ ,  $ZrO_2/CNT$ , and  $Nb_2O_5/CNT$  on the reaction route and product distribution of cellulose catalytic hydrogenation were studied in this paper.

## EXPERIMENTAL

### Materials

Microcrystalline cellulose,  $Ce(NO_3)_3 \cdot 6H_2O$ ,  $ZrO(NO_3)_2 \cdot 6H_2O$ ,  $NbCl_5$ ,  $Ni(NO_3)_2 \cdot 6H_2O$ ,  $Zn(NO_3)_2 \cdot 6H_2O$ , citric acid, EG, 1,2-PG, tetrahydrofuran dimethanol (THFDM), sorbitol, glucose, mannose, fructose, and 1,4-sorbitan were purchased from Sigma-Aldrich. They were all analytical reagents. Carbon nanotubes (CNT) were from Chengdu Organic Chemicals Co. Ltd, China.

### Preparation of Catalyst

To remove mineral impurities, CNT was pretreated with 65% nitric acid as previously described (Van der Wijst *et al.* 2015), briefly, boiled for 30 min, then washed with deionization water until the filtrate was neutral. A complex solution was composed by mixing the metal salt ( $Ce(NO_3)_3 \cdot 6H_2O$ ,  $ZrO(NO_3)_2 \cdot 6H_2O$ ,  $NbCl_5$ ,  $Ni(NO_3)_2 \cdot 6H_2O$ , or  $Zn(NO_3)_2 \cdot 6H_2O$ ), citric acid (CA), EG and deionized water in an ultrasonic bath for 10 min. The molar ratios between the three components Metal:CA:EG used were 7:8:8. The complex solution was introduced to the CNTs in isometric impregnation, with the ratio of 4.32 mmol metal to 1 g CNT. Metal salts/CNT precursor dried in room temperature for 12 h and at 110 °C for 12 h, then calcinated for 10 min at 400 °C in air flow to form metal oxide (MOx)/CNT. The heating and cooling were done in pure  $N_2$  flow with a heating rate of 10 °C/min. For NiO/CNT, reduction was carried out in  $H_2$  gas for 5 h at 400 °C to form Ni/CNT.

## Characterization of Catalyst

The contents of metal in the catalyst were determined by Inductively Coupled Plasma Optical Emission Spectrometry (ICP-OES) (Thermo IRIS intrepid II). 0.010 g of catalyst was dissolved in acid solution (40% HF for ZrO<sub>2</sub>/CNT and Nb<sub>2</sub>O<sub>5</sub>/CNT, 6 mol/L HNO<sub>3</sub> for CeO<sub>2</sub>/CNT, diluted HNO<sub>3</sub> for Ni/CNT and ZnO/CNT), digested for 60 min (90 °C for CeO<sub>2</sub>/CNT and ZrO<sub>2</sub>/CNT, 25 °C for other catalysts), and diluted with water to 25 mL. 1 mL of supernatant was taken, diluted to the second 25 mL, and the solution was collected for the detection. X-ray photoelectron spectroscopy (XPS) analyses were carried out with a PHI Quantera SXM X-ray photoelectron spectrometer using a monochromatic Al-Kα X-ray source. The phase structure of the catalyst was determined by powder X-ray diffraction (XRD) spectroscopy (Bruker D8 Advance) using a Cu-Kα radiation ( $k = 0.154$  nm), the data ranging from 5 to 80 were collected at a step size of 0.02, and the particle size was investigated using the Scherrer Equation. The surface morphology and structure of the catalyst was collected by transmission electron microscope (TEM) (HITACHI-HT 7700).

Surface acid (base) properties of the catalysts were probed by NH<sub>3</sub> (CO<sub>2</sub>)-Temperature Programmed Desorption (TPD), CO<sub>2</sub>-TPD was performed on a Cat-Lab instrument (BEL, Japan) equipped with a well-calibrated quadrupole mass spectrometer (MS) (Inprocess Instruments, GAM 200) as the detector. The CO<sub>2</sub> desorption profiles were obtained by recording the signal for molecular CO<sub>2</sub> ( $m/z=44$ ). NH<sub>3</sub>-TPD was performed on TPD-TPR instrument (Xianquan, China TP-5076) equipped with a TCD detector. The sample of 40 mg (50 mg) was purged with dry Ar (He) at 500 °C for 1 h, followed by reducing the reactor temperature to 100 °C (50 °C) and switching to a flow of 20% CO<sub>2</sub>/Ar (10% NH<sub>3</sub>/He) for 1 h to execute CO<sub>2</sub> (NH<sub>3</sub>) adsorption. After purging for 1.5 h at 100 °C (several minutes at 50 °C) with flowing Ar (He) until the signal was constant, the sample was heated to 500 °C at a rate of 10 °C min<sup>-1</sup>, then kept for 30 min (90 min) to allow for desorption of adsorbed CO<sub>2</sub> (NH<sub>3</sub>). MS intensity ratio of CO<sub>2</sub> to Ar and the volume of Ar passed were used to quantify the CO<sub>2</sub> desorption amounts. For NH<sub>3</sub>, the calibration was performed by injecting pulses of 10% NH<sub>3</sub>/He. The amounts of the acid and basic sites were analyzed based on mathematical deconvolution of the TPD profiles.

## Procedure for Cellulose Conversion

The catalytic reactions were tested in a stirring batch reactor (Parr Instruments Company). Typically, a 300 mL batch reactor was used with deionized water (100 mL), microcrystalline cellulose (1.00 g), catalyst (Ni/CNT+MO<sub>x</sub>/CNT with the amount of Ni and MO<sub>x</sub> to be 0.81 mmol) and an initial H<sub>2</sub> pressure of 60 bar. The reactor was closed and heated to  $T=245^{\circ}\text{C}$  with a heating rate of 2 °C/min, which generated a pressure of 120 bar, and the system was kept at  $T=245^{\circ}\text{C}$  for 270 min. When the temperature was ramped to 180, 210, and 240 °C, three samples were taken marked as 180C, 210C, and 240C. Alternatively, when the reaction went on for 15, 30, 45, 90, 150, 210, and 270 min at 245 °C, samples taken were marked as 15M, 30M, 45M, 90M, 150M, 210M, and 270M. After the reaction, the catalyst was retrieved from the reaction mixture using a quantitative ashless filter paper. The conversion of cellulose was calculated according to equation (1). The yields of product were calculated according to equation (2). The catalytic reactions were duplicated, the relative standard deviations of product yield were below 5% (yield>0.05).

$$\text{cellulose conversion} = \frac{W_{\text{cellulose added}} + W_{\text{catalyst added}} - W_{\text{residue}}}{W_{\text{cellulose added}}} \times 100\% \quad (1)$$

$$\text{Product yield: } Y = \frac{m_{\text{product}} \times (\text{mass fraction of carbon in product})}{m_{\text{cellulose}} \times (\text{mass fraction of carbon in cellulose})} \quad (2)$$

where  $W_{\text{cellulose added}}$  and  $W_{\text{catalyst added}}$  represent the weight (g) of cellulose and catalyst added,  $W_{\text{residue}}$  represents the weight (g) of residue retrieved, containing used catalyst,  $m_{\text{product}}$  represents the mass of product (g), for which the products were EG, 1,2-PG, sorbitol, THFDM, and 1,4-sorbitan,  $m_{\text{cellulose}}$  represents the mass of cellulose added (g).

### Analysis of Products

HPLC (Agilent Technologies 1260 Infinity)-RID (differential refractive index detector) with a Hi-Plex Ca (Duo) 300 x 6.5 mm column was used to quantitatively detect the product, the concentration of product was obtained by one-point external standard method with the content of standard solution below 0.4 mg/mL. The relative standard deviation of the analytical method was below 1% (yield >0.05). To monitor glucose and its isomer, SIM mode evaluations ( $m/z=203$ ) of all samples were conducted with a SHIMADZU LCMS 2010 EV.

## RESULTS AND DISCUSSION

### Characterization of the Catalyst

The contents of metal in catalysts were detected by ICP-OES. As shown in Table S-1, the contents were close to those calculated by the amount of reactant. They were from 2.29 to 3.05 mmol/g. The valences of metal in catalysts were identified by XPS spectrum (Fig S-1 to S-4). The binding energy of  $\text{Ce}_{3d}$  indicated that  $\text{CeO}_2$  and  $\text{Ce}_2\text{O}_3$  were coexistent, and other metal oxides were identified to be  $\text{ZnO}$ ,  $\text{Nb}_2\text{O}_5$ , and  $\text{ZrO}_2$ . The XRD patterns of catalyst are shown in Fig. 1.

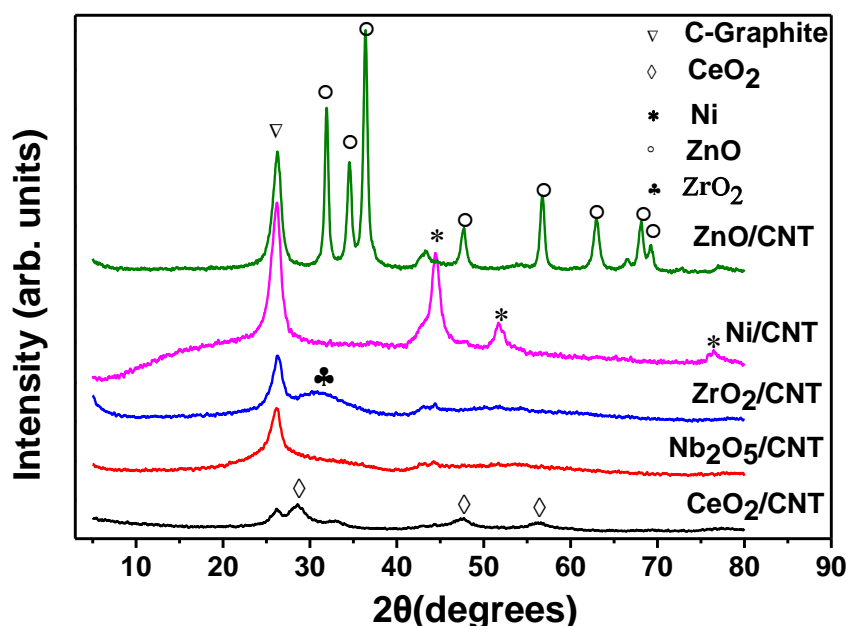
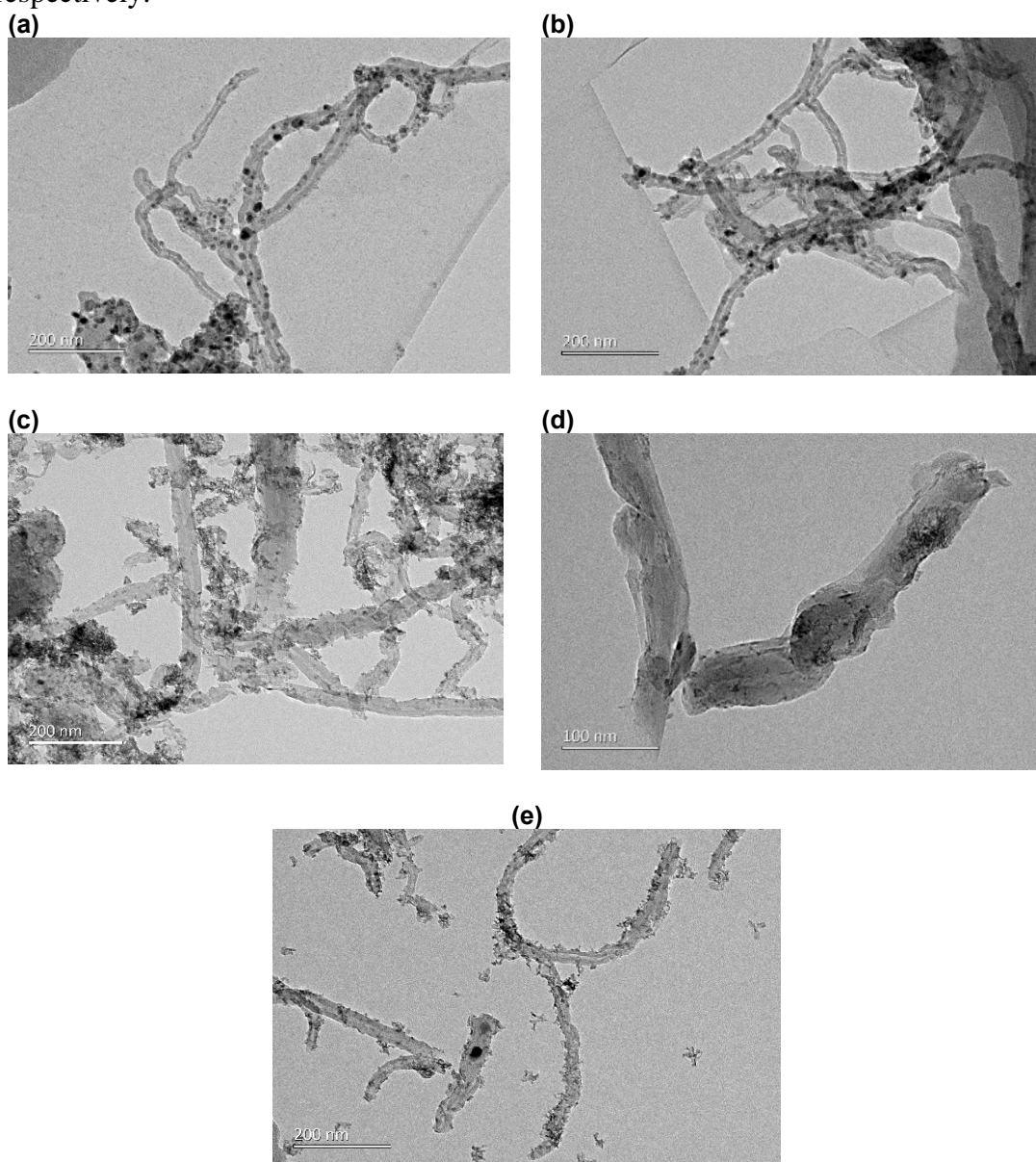


Fig. 1. XRD profile of the catalysts

Metal oxide diffraction peaks were observed in profile of Ni/CNT (Ni, cubic, PDF 00-004-0850), ZnO/CNT (ZnO, Hexagonal, PDF 01-075-0576), and CeO<sub>2</sub>/CNT (CeO<sub>2</sub>, cubic, PDF 01-075-0076). The particle size calculated by the Scherrer Equation were 12.4, 17.5, and 3.3 nm, respectively. No diffraction peaks for metal oxides were observed in profile of ZrO<sub>2</sub>/CNT and Nb<sub>2</sub>O<sub>5</sub>/CNT, indicating that ZrO<sub>2</sub> and Nb<sub>2</sub>O<sub>5</sub> were amorphous. The morphology of the catalysts was collected by TEM (Fig. 2). TEM images showed that the particle sizes of Ni, ZnO, CeO<sub>2</sub>, Nb<sub>2</sub>O<sub>5</sub>, and ZrO<sub>2</sub> were 14.5, 15.1, 5.7, 4.7, and 3.0 nm, respectively.



**Fig. 2.** TEM graph of the catalysts. (a). Ni/CNT; (b). ZnO/CNT; (c). CeO<sub>2</sub>/CNT; (d). ZrO<sub>2</sub>/CNT; (e). Nb<sub>2</sub>O<sub>5</sub>/CNT

TPD was performed to probe Lewis acid and base sites of the catalysts. Table 1, Fig. S-5, and Fig.S-6 show the acid (base) concentration and strength of different catalysts. The most abundant base sites were found in CeO<sub>2</sub>/CNT, including weak, medium, and strong in strength. A few weak, medium, and strong basic sites were found in ZnO/CNT.

Many weak and a few strong basic sites were found in ZrO<sub>2</sub>/CNT. Only strong basic sites in Nb<sub>2</sub>O<sub>5</sub>/CNT were observed. A wide distribution of surface base sites from weak to strong were probed in all four catalysts, but the abundance in CeO<sub>2</sub>/CNT was far more than in the other three catalysts.

**Table 1.** Concentration of Weak, Medium, and Strong Base and Acid Sites for Four Catalysts

Catalyst	Base sites ( $\mu\text{mol CO}_2 \text{ g}^{-1}$ )				Acid sites ( $\mu\text{mol NH}_3 \text{ g}^{-1}$ )			
	Weak	Medium	Strong	total	Weak	medium	strong	total
CeO <sub>2</sub> /CNT	8.55	9.28	12.64	30.47	5.41	5.23	13.39	24.03
ZrO <sub>2</sub> /CNT	4.35	-	2.62	6.97	2.95	0.60	0.50	4.05
Nb <sub>2</sub> O <sub>5</sub> /CNT	-	-	2.62	2.62	3.88	1.14	0.20	5.22
ZnO/CNT	0.36	0.51	1.27	2.14	0.86	-	1.20	2.06

Weak: Desorption temperatures below 200 °C. Medium: Desorption temperatures at 200–400 °C. Strong: Desorption temperatures above 400 °C.

## Product Distribution

### *The cellulose conversion*

The cellulose conversion was calculated based on the relative change of weight before and after the reaction. They were 100% for all four types of catalysts when the reaction time was 270 min. When the reaction time was 30 min, cellulose conversions were 70.0%, 75.7%, 79.1%, and 91.2% for ZrO<sub>2</sub>/CNT, CeO<sub>2</sub>/CNT, Nb<sub>2</sub>O<sub>5</sub>/CNT, and ZnO/CNT.

### *Glucose and its isomerization*

Isomerization have been demonstrated to take place in hot compressed water (Lu *et al.* 2012; Yan *et al.* 2021), Lewis acids such as metal salt (Nguyen *et al.* 2016), heterogeneous metal-substituted BEA zeolites (Gounder and Davis 2013; Bermejo-Deval *et al.* 2014), alkaline solution (Speck 1958), and various other media (Nagorski and Richard 2001; Saravanamurugan and Riisager 2014; Murzin *et al.* 2017). 1,2-hydride transfer and 1,5-hydride transfer of glucose were observed in the Lewis Acid solution (Gounder and Davis 2013; Nguyen *et al.* 2016), to form fructose and sorbose, respectively.

In light of their low concentrations and overlap with the corresponding values for of other substances in liquid chromatography, glucose and its isomers were detected by MS signals with  $m/z=203$ . The results are shown in Fig. 3 and Table S-2. There were three main isomers: glucose (Retention Time (Rt)=18.94), mannose (Rt=21.15), and fructose (Rt=22.48). No sorbose or galactose were detected. Mannose could be an inverse isomerization product of fructose. No mannose was detected with the catalyst CeO<sub>2</sub>/CNT. Two new peaks (Rt=25.10 and 26.45) were observed with the catalyst CeO<sub>2</sub>/CNT and Nb<sub>2</sub>O<sub>5</sub>/CNT, for which the Rt corresponded to tagatose and an unknown substance.

Hexoses were increased in the former stage of the reaction and decreased later. Little hexose was detected at the end of reaction. The concentration of glucose varied greatly in reactions using different catalysts. The highest was in ZrO<sub>2</sub>/CNT (reaction time=30 min; yield<0.005), followed by Nb<sub>2</sub>O<sub>5</sub>/CNT and ZnO/CNT, and the lowest was in CeO<sub>2</sub>/CNT. The strength and amount of surface acid and base site could accelerate the consumption of glucose. The CeO<sub>2</sub>/CNT was found to possess a large amount of strong acid and base sites, leading to the lowest hexose concentration. Glucose was isomerized partially to fructose in ZnO/CNT and CeO<sub>2</sub>/CNT.

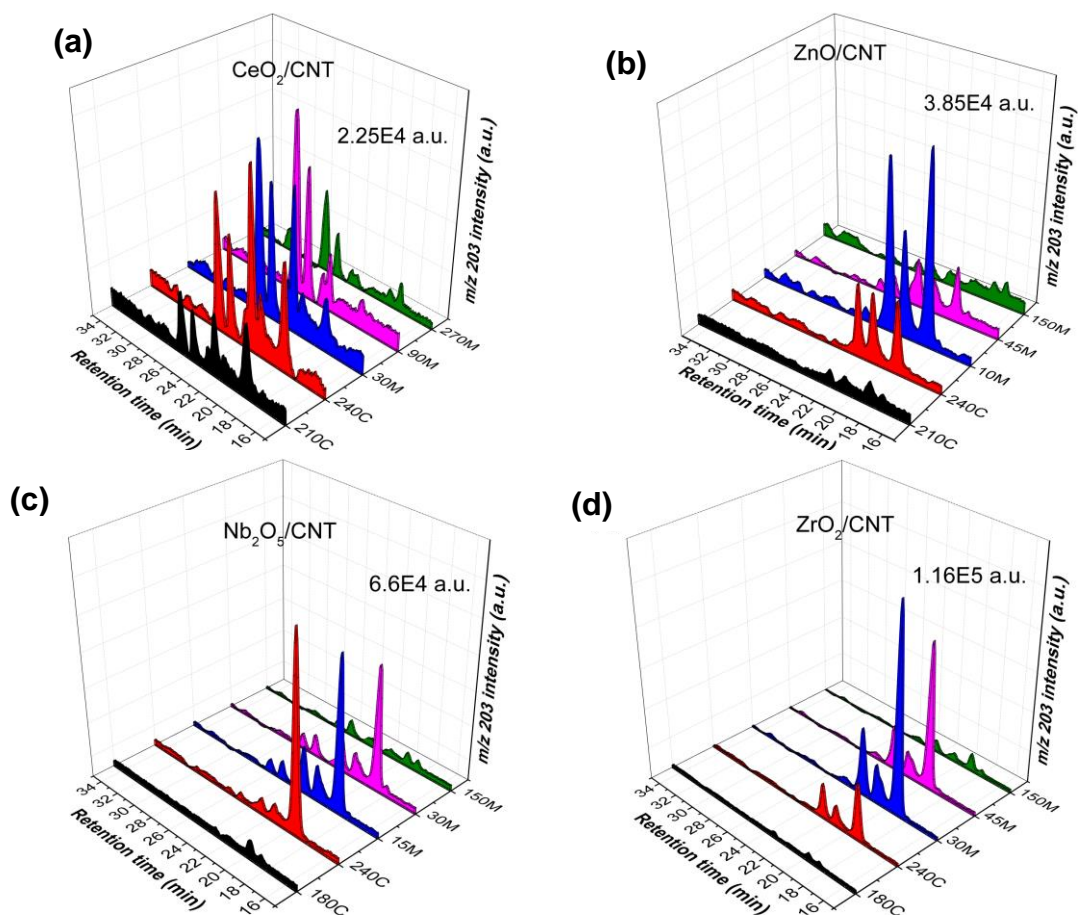


**Fig. 3.** LC-MS ( $m/z=203$ ) of samples in different reaction time. (a) CeO<sub>2</sub>, Rt=19.21, 21.76, 22.65, 25.10 and 26.45 min. (b) ZnO, Rt= 18.94, 21.15 and 22.48 min. (c) Nb<sub>2</sub>O<sub>5</sub>, Rt=18.87, 21.15, 22.41, 24.70 and 26.07 min. (d) ZrO<sub>2</sub>, Rt=18.91, 21.08 and 22.49 min

#### Yield variation of main products in reaction time

The yield variations of sorbitol, EG, 1,2-PG, THFDM, and 1,4-sorbitan in reaction time with different catalysts are shown in Fig. 4.

The yields of sorbitol increased at the former stage of the reaction, but decreased as time went on for all four catalysts. The optimal reaction time was 90 min for sorbitol. The highest sorbitol yield was 31.1%, obtained for ZrO<sub>2</sub>/CNT at 90 min. Sorbitol yields were in the range of 16.8 to 53.4%, when carbon blacks, activated carbon, Al<sub>2</sub>O<sub>3</sub>, ZrO<sub>2</sub>, or TiO<sub>2</sub> supported Pt catalyst were employed (Kobayashi *et al.* 2011). In systems where acid-functionalized carbonaceous materials or HZSM-5 served as support, and where Pt, Ru, or Ni served as the active component, the sorbitol yields were in the range of 39.4 to 70.0% (Manaenkov *et al.* 2019). A sorbitol yield of 91.0% was obtained with CuO/CeO<sub>2</sub>-ZrO<sub>2</sub> (Manaenkov *et al.* 2019). Sorbitol could be decreased by dehydrogenation (Deutsch *et al.* 2012; Jia and Liu 2016), dehydration (Sun *et al.* 2013), hydrogenolysis (Sun *et al.* 2015), *etc.*

The yields of EG increased at the former stage of the reaction, and they kept constant for ZrO<sub>2</sub>/CNT, ZnO/CNT, and Nb<sub>2</sub>O<sub>5</sub>/CNT after 90 min, but decreased for CeO<sub>2</sub>/CNT after 150 min. The highest EG yield was 36.3%, obtained for CeO<sub>2</sub>/CNT at 150 min. It is widely accepted that W-containing catalysts have the tendency of producing high

EG yields. The EG yields by using of many W-containing catalysts were reviewed; they were in the range of 8.4 to 77.5% (Manaenkov *et al.* 2019).

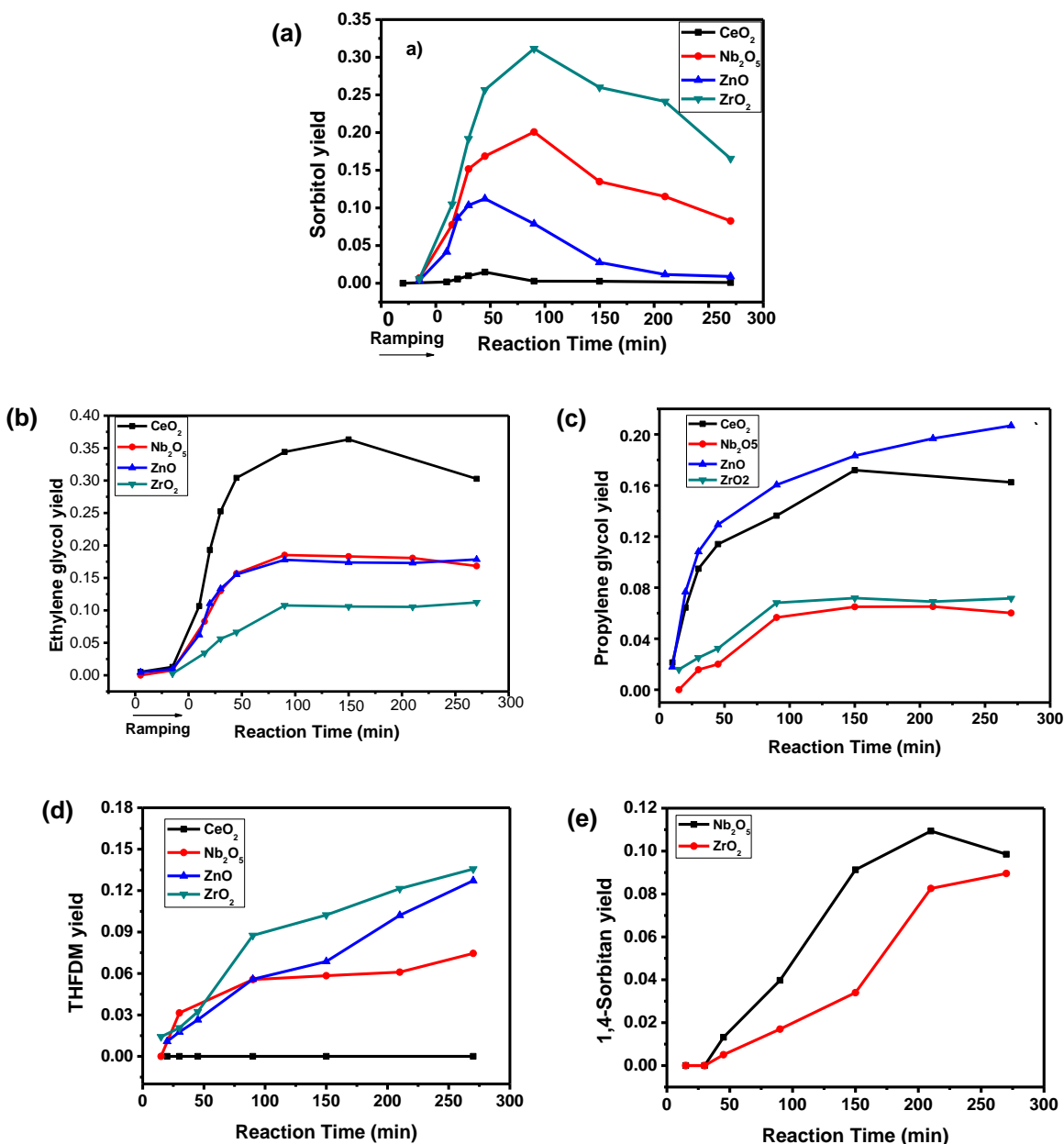


**Fig. 4.** The yields of some products in different reaction time. Reaction conditions:  $P = 60$  bars,  $H_2$  at room temperature (RT),  $T = RT$  to  $245$  °C with a heating rate of  $2$  °C /min, kept at  $245$  °C for 270 min. Microcrystalline cellulose (1.00 g), catalyst ((Ni/CNT+ $MO_x$ /CNT with Ni and  $MO_x$  to be 0.81 mmol) and distilled water (100 mL) in a 300 mL autoclave reactor.

The yields of 1,2-PG increased at the former stage of the reaction, and kept constant for  $ZrO_2$ /CNT and  $Nb_2O_5$ /CNT after 90 min, kept increased for  $ZnO$ /CNT after 90 min, and decreased for  $CeO_2$ /CNT after 150 min. The highest 1,2-PG yield was 20.7%, obtained for  $ZnO$ /CNT at 270 min. High 1,2-PG yields were obtained in CuCr catalysts (Xiao *et al.* 2013) and Sn-containing catalysts (Manaenkov *et al.* 2019); the yields were in the range of 32.2 to 39.0%.

The yields of THFDM kept increasing all the time for ZnO/CNT, Nb<sub>2</sub>O<sub>5</sub>/CNT, and ZrO<sub>2</sub>/CNT. The rate of increase for ZnO/CNT was higher than those for Nb<sub>2</sub>O<sub>5</sub>/CNT and ZrO<sub>2</sub>/CNT after 150 min. No THFDM was detected for CeO<sub>2</sub>/CNT. The highest yield was 13.6%, obtained for ZrO<sub>2</sub>/CNT at 270 min. Niobic acid and a ruthenium catalyst were used in glucose conversion, the selectivity to THFDM was 60% and conversion was 49% (Duan *et al.* 2017). 1,4-sorbitan was only observed for Nb<sub>2</sub>O<sub>5</sub>/CNT and ZrO<sub>2</sub>/CNT, the yields were 10.9% and 9.0%, respectively. Layered niobium molybdate (HNbMoO<sub>6</sub>) (Morita *et al.* 2014) and sulfuric acid (Yabushita *et al.* 2015) were used in the dehydration of aqueous-phase sorbitol, where the yields of 1,4-sorbitan were 33% and 58% respectively. The yields of 1,4-sorbitan kept increasing continually, except for a decline for Nb<sub>2</sub>O<sub>5</sub>/CNT after 210 min. The dehydration of sorbitol to 1,4-sorbitan was an acid-catalyzed reaction (Sun *et al.* 2013).

## Discussion

The yields of EG, 1,2-PG, sorbitol, and sorbitans were mainly influenced by several types of reaction, as shown in Fig. 5. RAC of glucose produces EG. RAC of fructose produces 1,2-PG. Hydrogenation of glucose produces sorbitol. Dehydration of sorbitol produces 1,4-sorbitan, isosorbitan, and THFDM. Dehydration of fructose produces hydroxymethylfurfural (HMF) (Aida *et al.* 2007). The HMF is then hydrogenated to THFDM.

ZnO/CNT resulted in the fastest cellulose hydrolysis rate. The isomerization of glucose to fructose (consumption of product) helped the hydrolysis reaction going forward. For CeO<sub>2</sub>/CNT, though the glucose consumption was fastest, glucose experienced C-C bond cracking, resulting in many small molecules, which occupied active H<sup>+</sup> and active sites. These effects tempered the cellulose hydrolysis. No glucose or fructose was detected after 90 min for all four catalysts, which implied that cellulose hydrolysis had completed at 90 min.

The yields of EG and 1,2-PG were increased for CeO<sub>2</sub>/CNT from 90 min to 150 min. This effect could have originated from RAC of pentose, or terminal C-C scission of glyceraldehyde or erythrose. Glucose could be oxidized to gluconic acid for the ability of CeO<sub>x</sub> to shuttle between Ce(III) and Ce(IV) state (Montini *et al.* 2016), then decarboxylation took place (Bohre *et al.* 2019), generating terminal C-C scission. Parts of EG and 1,2-PG were hydrodeoxygenated to ethanol and propanol after 150 min.

For ZnO/CNT, sorbitol decreased, EG kept constant, and 1,2-PG increased after 90 min, which demonstrated that sorbitol was dehydrogenated at the 2/5-position, not the 1,6-position, which in accordance with the conclusion that a sorbitol dehydrogenation step proceeded by preferential activation of its C (5)-H bond (Jia and Liu 2016).

For Nb<sub>2</sub>O<sub>5</sub>/CNT and ZrO<sub>2</sub>/CNT, EG and 1,2-PG were constant after 90 min, which implied that dehydrogenation of sorbitol was hard to achieve. The increasing rate of THFDM yield was lower after 90 min, which disclosed that the reaction rate of fructose to THFDM was faster than sorbitol to THFDM. Parts of 1,4-sorbitan had been converted to isosorbitan for Nb<sub>2</sub>O<sub>5</sub>/CNT after 210 min.

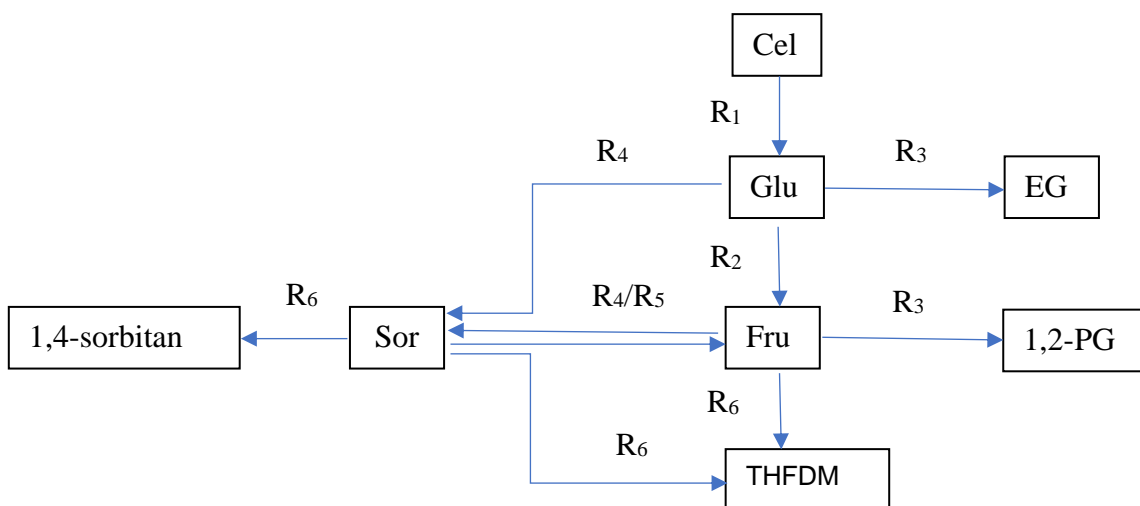


**Fig. 5.** Main reaction routes for cellulose hydrothermal hydrogenolysis. (Cel: Cellulose; Glu: Glucose; Fru: Fructose; THFDM: tetrahydrofuran dimethanol; Sor: Sorbitol; EG: Ethylene glycol; 1,2-PG: Propylene glycol. R<sub>1</sub>: hydrolysis; R<sub>2</sub>: isomerization; R<sub>3</sub>: retro-aldol condensation; R<sub>4</sub>: hydrogenation; R<sub>5</sub>: dehydrogenation; R<sub>6</sub>: dehydration).

Less EG and 1,2-PG were produced for Nb<sub>2</sub>O<sub>5</sub>/CNT and ZrO<sub>2</sub>/CNT. 23.9% EG and 7.4% 1,2-PG were formed by Ni/CNT alone in the authors' previous study (Van der Wijst *et al.* 2015). Nb<sub>2</sub>O<sub>5</sub>/CNT and ZrO<sub>2</sub>/CNT were found to be inert to C-C bond cracking. Liu's studies showed that the crystallized WO<sub>3</sub> was essential to C-C scission (Liu *et al.* 2012, 2022). Nb<sub>2</sub>O<sub>5</sub>/CNT and ZrO<sub>2</sub>/CNT were amorphous, which may cause inertness. However, in Gromov's study, the main product of cellulose hydrogenolysis on hexagonal Nb<sub>2</sub>O<sub>5</sub> and on monoclinic or tetragonal ZrO<sub>2</sub> was also sorbitol (Gromov *et al.* 2021). It follows that the inertness of Nb<sub>2</sub>O<sub>5</sub>/CNT and ZrO<sub>2</sub>/CNT could be attributed to the surface acid/base property.

## CONCLUSIONS

1. The supported catalyst CeO<sub>2</sub>/carbon nanotube (CNT) was found to be rich in strong Lewis acid and base sites, and the crystallized CeO<sub>2</sub> was redox active. In addition, it was active in C-C bond cracking (retro-aldol condensation (RAC), terminal C-C scission), isomerization, dehydrogenation, and hydrodeoxygenation reactions. The reaction yielded 36.3% ethylene glycol (EG) and 17.2% 1,2-propylene glycol (1,2-PG).
2. ZnO/CNT with Brønsted base accelerates isomerization, RAC, and dehydrogenation, yielding 20.7% 1,2-PG, 17.8% EG, and 12.7% THFDM.
3. Nb<sub>2</sub>O<sub>5</sub>/CNT and ZrO<sub>2</sub>/CNT were found to be inert to C-C bond cracking, H<sup>+</sup> in hot compressed water and the Brønsted acid in Nb<sub>2</sub>O<sub>5</sub>/CNT accelerated dehydration, yielding more sorbitol and sorbitan.
4. The reaction network for cellulose hydrogenolysis is complex. The type of metal oxides influences glucose evolution and final product distribution greatly. Reaction time and catalysts should be cautiously selected to get a certain product.

## ACKNOWLEDGMENTS

The authors thank Prof. Boqing Xu and Dr. Zonghui Liu of Department of Chemistry, Tsinghua University for the help in CO<sub>2</sub>-TPD experiment, Ms. Peipei Li for the collection of HPLC-MS data, Dr. Jiying Wei, Dr. Hongrui Liu, Dr. Cornelis van der Wijst, and Dr. Haakon M. Rui for helpful discussion.

This work was supported by Research Council of Norway (Project No: 263868/H30); National Key R&D Program of China (2016YFE0108500), National Natural Science Foundation of China (No. 21838006).

## REFERENCES CITED

- Aida, T. M., Tajima, K., Watanabe, M., Saito, Y., Kuroda, K., Nonaka, T., Hattori, H., Smith, R. L., and Arai, K. (2007). "Reactions of D-fructose in water at temperatures up to 400 degrees C and pressures up to 100 MPa," *Journal of Supercritical Fluids* 42(1), 110-119. DOI: 10.1016/j.supflu.2006.12.017
- Bermejo-Deval, R., Orazov, M., Gounder, R., Hwang, S. J., and Davis, M. E. (2014). "Active sites in Sn-beta for glucose isomerization to fructose and epimerization to mannose," *ACS Catalysis* 4(7), 2288-2297. DOI: 10.1021/cs500466j
- Bohre, A., Hocevar, B., Grilc, M., and Likozar, B. (2019). "Selective catalytic decarboxylation of biomass-derived carboxylic acids to bio-based methacrylic acid over hexaaluminate catalysts," *Applied Catalysis B-Environmental* 256. DOI: 10.1016/j.apcatb.2019.117889
- Chen, Y., Mu, R., Yang, M., Fang, L., Wu, Y., Wu, K., Liu, Y., and Gong, J. (2017). "Catalytic hydrothermal liquefaction for bio-oil production over CNTs supported metal catalysts." *Chemical Engineering Science*, 161, 299-307. DOI: 10.1016/j.ces.2016.12.010
- Delidovich, I., and Palkovits, R. (2016). "Catalytic isomerization of biomass-derived aldoses: A review," *Chemsuschem* 9(6), 547-561. DOI: 10.1002/cssc.201501577
- Deutsch, K. L., Lahr, D. G., and Shanks, B. H. (2012). "Probing the ruthenium-catalyzed higher polyol hydrogenolysis reaction through the use of stereoisomers," *Green Chemistry* 14(6) 1635-1642. DOI: 10.1039/c2gc00026a
- Duan, Y., Zhang, J., Li, D., Deng, D., Ma, L.-F., and Yang, Y. (2017). "Direct conversion of carbohydrates to diol by the combination of niobic acid and a hydrophobic ruthenium catalyst." *RSC Advances* 7(42), 26487-26493. DOI: 10.1039/c7ra03939e
- Gounder, R., and Davis, M. E. (2013). "Titanium-beta zeolites catalyze the stereospecific isomerization of D-glucose to L-sorbose via intramolecular C5-C1 hydride shift," *ACS Catalysis* 3(7), 1469-1476. DOI: 10.1021/cs400273c
- Gromov, N. V., Medvedeva, T. B., Rodikova, Y. A., Timofeeva, M. N., Panchenko, V. N., Taran, O. P., Kozhevnikov, I. V., and Parmon, V. N. (2021). "One-pot synthesis of sorbitol via hydrolysis-hydrogenation of cellulose in the presence of Ru-containing composites," *Bioresource Technology* 319. DOI: 10.1016/j.biortech.2020.124122
- Gu, M. Y., Shen, Z., Yang, L., Dong, W. J., Kong, L., Zhang, W., Peng, B. Y., and Zhang, Y. L. (2019). "Reaction route selection for cellulose hydrogenolysis into C-2/C-3 glycols by ZnO-modified Ni-W/beta-zeolite catalysts," *Scientific Reports* 9.

- DOI: 10.1038/s41598-019-48103-6
- Huang, J. C., Wang, W., Li, D. F., Xu, S., Liu, Q., Chen, X., Fei, Z. Y., Zhang, Z. X., Cui, M. F., Tang, J. H., and Qiao, X. (2019). "Facile construction of non-crystalline ZrO<sub>2</sub> as an active yet durable catalyst for methane oxychlorination," *Journal of Sol-Gel Science and Technology* 92(1), 163-172. DOI: 10.1007/s10971-019-05089-x
- Jia, Y. Q., and Liu, H. C. (2016). "Mechanistic insight into the selective hydrogenolysis of sorbitol to propylene glycol and ethylene glycol on supported Ru catalysts," *Catalysis Science & Technology* 6(19), 7042-7052. DOI: 10.1039/c6cy00928j
- Kobayashi, H., Ito, Y., Komanoya, T., Hosaka, Y., Dhepe, P. L., Kasai, K., Hara, K., and Fukuoka, A. (2011). "Synthesis of sugar alcohols by hydrolytic hydrogenation of cellulose over supported metal catalysts," *Green Chemistry* 13(2), 326-333. DOI: 10.1039/c0gc00666a
- Kosmulski, M. (1997). "Attempt to determine pristine points of zero charge of Nb<sub>2</sub>O<sub>5</sub>, Ta<sub>2</sub>O<sub>5</sub>, and HfO<sub>2</sub>," *Langmuir* 13(23), 6315-6320. DOI: 10.1021/la970469g
- Lazaridis, P. A., Karakoulia, S. A., Teodorescu, C., Apostol, N., Macovei, D., Panteli, A., Delimitis, A., Coman, S. M., Parvulescu, V. I., and Triantafyllidis, K. S. (2017). "High hexitols selectivity in cellulose hydrolytic hydrogenation over platinum (Pt) vs. ruthenium (Ru) catalysts supported on micro/mesoporous carbon," *Applied Catalysis B-Environmental* 214, 1-14. DOI: 10.1016/j.apcatb.2017.05.031
- Li, C., Xu, G. Y., Li, K., Wang, C. G., Zhang, Y., and Fu, Y. (2019). "A weakly basic Co/CeO<sub>x</sub> catalytic system for one-pot conversion of cellulose to diols: Kungfu on eggs," *Chemical Communications* 55(53), 7663-7666. DOI: 10.1039/c9cc04020j
- Li, N., Ji, Z., Wei, L., Zheng, Y., Shen, Q., Ma, Q., Tan, M., Zhan, M., and Zhou, J. (2018). "Effect of the surface acid sites of tungsten trioxide for highly selective hydrogenation of cellulose to ethylene glycol," *Bioresource Technology* 264, 58-65. DOI: 10.1016/j.biortech.2018.05.026
- Li, N. X., Zheng, Y., Wei, L. F., Tenga, H. C., and Zhou, J. C. (2017). "Metal nanoparticles supported on WO<sub>3</sub> nanosheets for highly selective hydrogenolysis of cellulose to ethylene glycol," *Green Chemistry* 19(3), 682-691. DOI: 10.1039/c6gc01327a
- Li, Y. P., Liao, Y. H., Cao, X. F., Wang, T. J., Ma, L. L., Long, J. X., Liu, Q. Y., and Xua, Y. (2015). "Advances in hexitol and ethylene glycol production by one-pot hydrolytic hydrogenation and hydrogenolysis of cellulose," *Biomass & Bioenergy* 74, 148-161. DOI: 10.1016/j.biombioe.2014.12.025
- Liu, Y., Luo, C., and Liu, H. (2012). "Tungsten trioxide promoted selective conversion of cellulose into propylene glycol and ethylene glycol on a ruthenium catalyst," *Angewandte Chemie-International Edition* 51(13), 3249-3253. DOI: 10.1002/anie.201200351
- Liu, Y., Zhang, W., Hao, C., Wang, S., and Liu, H. (2022). "Unveiling the mechanism for selective cleavage of C-C bonds in sugar reactions on tungsten trioxide-based catalysts," *Proceedings of the National Academy of Sciences of the United States of America* 119(34). DOI: 10.1073/pnas.2206399119
- Liu, Z., and Liu, Z. (2020). "Comparison of hydrochar- and pyrochar-based solid acid catalysts from cornstalk: Physicochemical properties, catalytic activity and deactivation behavior," *Bioresource Technology* 297. DOI: 10.1016/j.biortech.2019.122477
- Lu, X., and Saka, S. (2012). "New insights on monosaccharides' isomerization, dehydration and fragmentation in hot-compressed water," *Journal of Supercritical*

- Fluids* 61, 146-156. DOI: 10.1016/j.supflu.2011.09.005
- Manaenkov, O. V., Kislitsa, O. V., Matveeva, V. G., Sulman, E. M., Sulman, M. G., and Bronstein, L. M. (2019). "Cellulose conversion into hexitols and glycols in water: Recent advances in catalyst development," *Frontiers in Chemistry* 7. DOI: 10.3389/fchem.2019.00834
- Maruani, V., Narayanin-Richenapin, S., Framery, E., and Andrioletti, B. (2018). "Acidic hydrothermal dehydration of D-glucose into humins: Identification and characterization of intermediates," *ACS Sustainable Chemistry & Engineering* 6(10), 13487-13493. DOI: 10.1021/acssuschemeng.8b03479
- Montini, T., Melchionna, M., Monai, M., and Fornasiero, P. (2016). "Fundamentals and catalytic applications of CeO<sub>2</sub>-based materials," *Chemical Reviews* 116(10), 5987-6041. DOI: 10.1021/acs.chemrev.5b00603
- Morita, Y., Furusato, S., Takagaki, A., Hayashi, S., Kikuchi, R., and Oyama, S. T. (2014). "Intercalation-controlled cyclodehydration of sorbitol in water over layered-niobium- molybdate solid acid," *Chemsuschem* 7(3), 748-752. DOI: 10.1002/cssc.201300946
- Murzin, D. Y., Murzina, E. V., Aho, A., Kazakova, M. A., Selyutin, A. G., Kubicka, D., Kuznetsov, V. L., and Simakova, I. L. (2017). "Aldose to ketose interconversion: galactose and arabinose isomerization over heterogeneous catalysts," *Catalysis Science & Technology* 7(22), 5321-5331. DOI: 10.1039/c7cy00281e
- Nagorski, R. W., and Richard, J. P. (2001). "Mechanistic imperatives for aldose-ketose isomerization in water: Specific, general base- and metal ion-catalyzed isomerization of glyceraldehyde with proton and hydride transfer," *Journal of the American Chemical Society* 123(5), 794-802. DOI: 10.1021/ja003433a
- Nguyen, H., Nikolakis, V., and Vlachos, D.G. (2016). "Mechanistic insights into Lewis Acid metal salt-catalyzed glucose chemistry in aqueous solution," *ACS Catalysis* 6(3), 1497-1504. DOI: 10.1021/acscatal.5b02698
- Pham, H. N., Anderson, A. E., Johnson, R. L., Schwartz, T. J., O'Neill, B. J., Duan, P., Schmidt-Rohr, K., Dumesic, J. A., and Datye, A. K. (2015). "Carbon overcoating of supported metal catalysts for improved hydrothermal stability," *ACS Catalysis* 5(8), 4546-4555. DOI:10.1021/acscatal.5b00329
- Saravanamurugan, S., and Riisager, A. (2014). "Zeolite-catalyzed isomerization of tetroses in aqueous medium," *Catalysis Science & Technology* 4(9), 3186-3190. DOI: 10.1039/c4cy00205a
- Shrotri, A., Kobayashi, H., and Fukuoka, A. (2018). "Cellulose depolymerization over heterogeneous catalysts," *Accounts of Chemical Research* 51(3), 761-768. DOI: 10.1021/acs.accounts.7b00614
- Speck, J. C. (1958). "The Lobry Debruyn-Alberda Vanekenstein transformation," *Advances in Carbohydrate Chemistry* 13, 63-103. WOS: A1958WM86200002
- Sun, P., Long, X. D., He, H., Xia, C. G., and Li, F. W. (2013). "Conversion of cellulose into isosorbide over bifunctional ruthenium nanoparticles supported on niobium phosphate," *Chemsuschem* 6(11), 2190-2197. DOI: 10.1002/cssc.201300701
- Sun, R. Y., Wang, T. T., Zheng, M. Y., Deng, W. Q., Pang, J. F., Wang, A. Q., Wang, X. D., and Zhang, T. (2015). "Versatile nickel-lanthanum(III) catalyst for direct conversion of cellulose to glycols," *ACS Catalysis* 5(2), 874-883. DOI: 10.1021/cs501372m
- Sun, R. Y., Zheng, M. Y., Pang, J. F., Liu, X., Wang, J. H., Pan, X. L., Wang, A. Q., Wang, X. D., and Zhang, T. (2016). "Selectivity-switchable conversion of cellulose

- to glycols over Ni-Sn catalysts,” *ACS Catalysis* 6(1), 191-201. DOI: 10.1021/acscatal.5b01807
- van der Wijst, C., Duan, X., Liland, I. S., Walmsley, J. C., Zhu, J., Wang, A., Zhang, T., and Chen, D. (2015). “ZnO-carbon-nanotube composite supported nickel catalysts for selective conversion of cellulose into vicinal diols,” *Chemcatchem* 7(18), 2991-2999. DOI: 10.1002/cctc.201500486
- Xiao, Z., Jin, S., Pang, M., and Liang, C. (2013). “Conversion of highly concentrated cellulose to 1,2-propanediol and ethylene glycol over highly efficient CuCr catalysts,” *Green Chemistry* 15(4), 891-895. DOI: 10.1039/c3gc40134k
- Yabushita, M., Kobayashi, H., Shrotri, A., Hara, K., Ito, S., and Fukuoka, A. (2015). “Sulfuric acid-catalyzed dehydration of sorbitol: mechanistic study on preferential formation of 1,4-sorbitan,” *Bulletin of the Chemical Society of Japan* 88(7), 996-1002. DOI: 10.1246/bcsj.20150080
- Yan, Z., Lian, J., Feng, Y., Li, M., Long, F., Cheng, R., Shi, S., Guo, H., and Lu, J. (2021). “A mechanistic insight into glucose conversion in subcritical water: Complex reaction network and the effects of acid-base catalysis,” *Fuel* 289. DOI: 10.1016/j.fuel.2020.119969
- Zan, Y. F., Miao, G., Wang, H., Kong, L. Z., Ding, Y. P., and Sun, Y. H. (2019). “Revealing the roles of components in glucose selective hydrogenation into 1,2-propanediol and ethylene glycol over Ni-MnOx-ZnO catalysts,” *Journal of Energy Chemistry* 38, 15-19. DOI: 10.1016/j.jechem.2018.12.016
- Zhang, K., Yang, G. H., Lyu, G. J., Jia, Z. X., Lucia, L. A., and Chen, J. C. (2019). “One-pot solvothermal synthesis of graphene nanocomposites for catalytic conversion of cellulose to ethylene glycol,” *ACS Sustainable Chemistry & Engineering* 7(13), 11110-11117. DOI: 10.1021/acssuschemeng.9b00006
- Zheng, M. Y., Pang, J. F., Sun, R. Y., Wang, A. Q., and Zhang, T. (2017). “Selectivity control for cellulose to diols: Dancing on eggs,” *ACS Catalysis* 7(3), 1939-1954. DOI: 10.1021/acscatal.6b03469

Article submitted: July 28, 2023; Peer review completed: August 19, 2023; Revised version received and accepted: August 30, 2023; Published: September 8, 2023.  
DOI: 10.15376/biores.18.4.7367-7390

## APPENDIX

Table S-1. Metal Content of Catalysts

Catalysts	Metal Content <sup>a</sup> (mmol/g)	Metal Content <sup>b</sup> (mmol/g)	Ratio (b/a)
Ni/CNT	3.25	3.05	0.94
CeO <sub>2</sub> /CNT	2.48	2.29	0.92
ZrO <sub>2</sub> /CNT	2.82	2.37	0.84
Nb <sub>2</sub> O <sub>5</sub> /CNT	2.75	2.46	0.89
ZnO/CNT	3.20	2.92	0.91

<sup>a</sup> means metal content calculated by the amount of adding. <sup>b</sup> means metal content detected by ICP-OES.

Table S-2. MS (m/z=203) Peak Area of Samples

Catalysts	Glucose Peak Area				
	180C	240C	15M	30M	45M
CeO <sub>2</sub> /CNT	-	404294	265376	133285	-
Nb <sub>2</sub> O <sub>5</sub> /CNT	126647	2089765	1523861	1301997	1356869
ZrO <sub>2</sub> /CNT	50191	1014821	3446931	3699475	2526217
ZnO/CNT	-	498434	1263747	881790	266261

Catalysts	Fructose Peak Area				
	180C	240C	15M	30M	45M
CeO <sub>2</sub> /CNT	-	695247	395240	392575	272952
Nb <sub>2</sub> O <sub>5</sub> /CNT	-	226605	495121	463051	488526
ZrO <sub>2</sub> /CNT	-	563771	1379152	1310923	883998
ZnO/CNT	-	476620	1197794	837857	345643

Catalysts	Mannose Peak Area				
	180C	240C	15M	30M	45M
CeO <sub>2</sub> /CNT	-	-	-	-	-
Nb <sub>2</sub> O <sub>5</sub> /CNT	-	293616	212858	365254	379649
ZrO <sub>2</sub> /CNT	-	376379	977200	915544	604114
ZnO/CNT	-	522400	816764	608119	189402

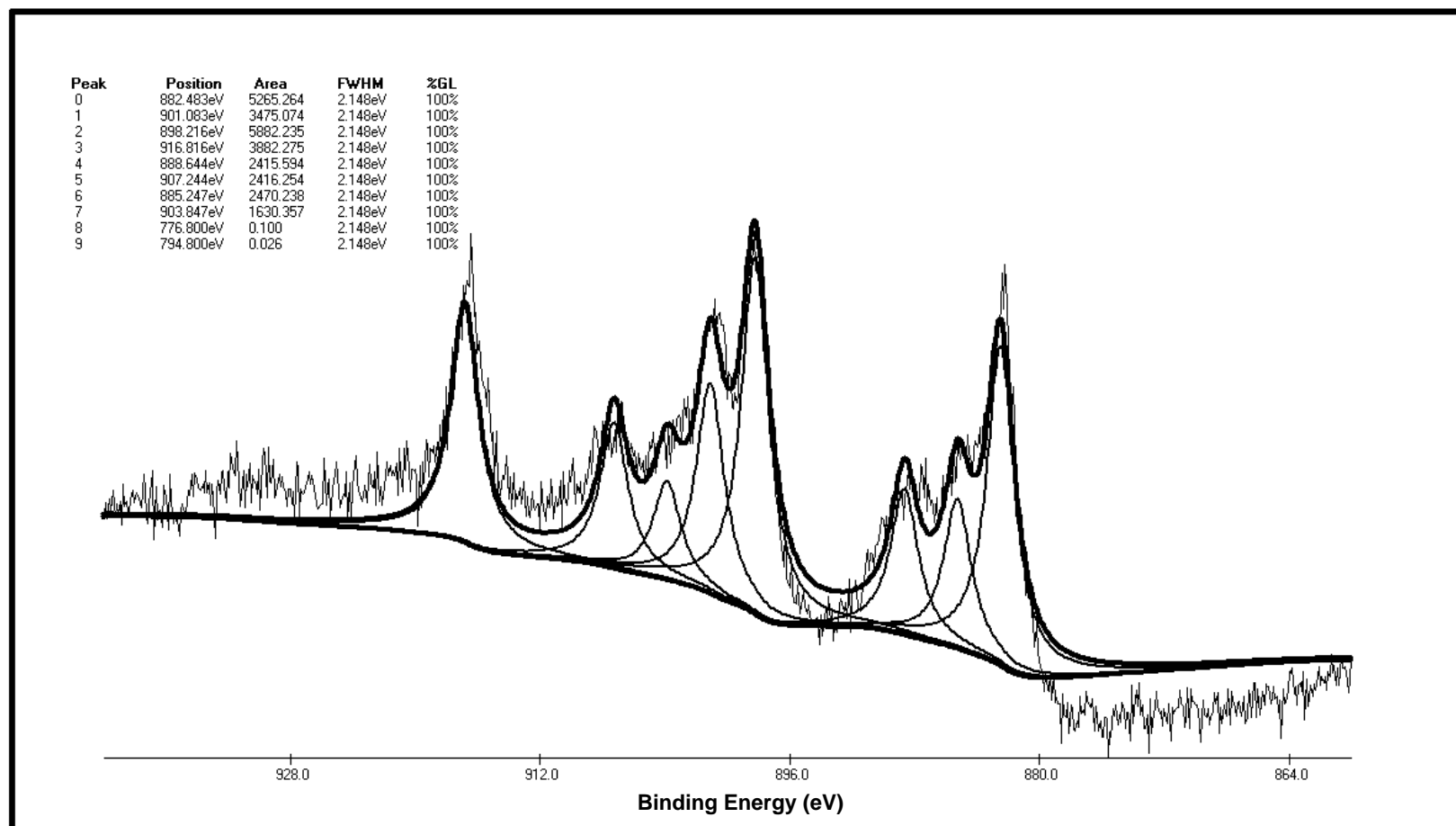


Fig. S-1. Binding energy of Ce<sub>3d</sub> of Ce (IV)O<sub>2</sub>+Ce<sub>2</sub>(III)O<sub>3</sub>/CNT

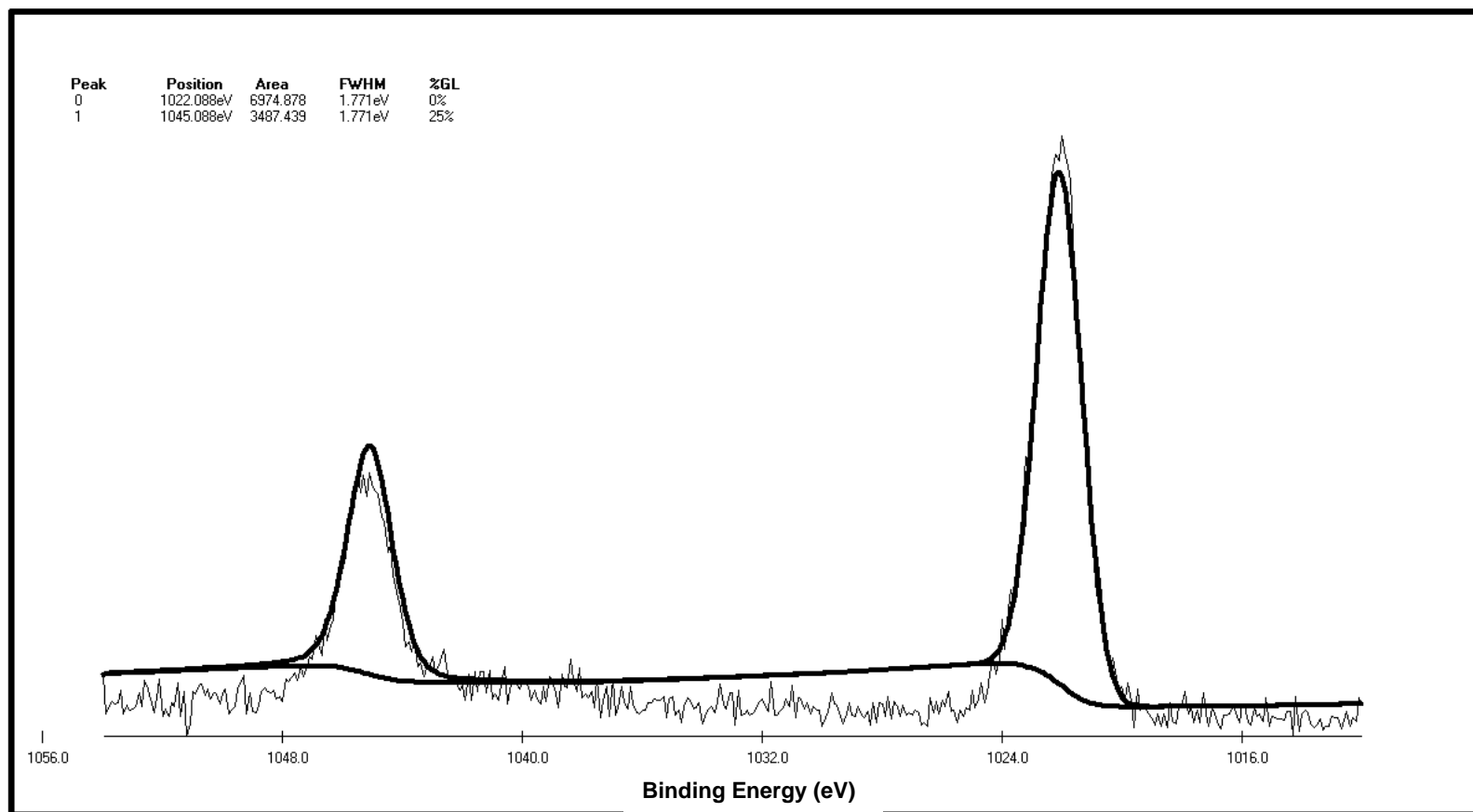


Fig. S-2. Binding energy of Zn<sub>2p</sub> of ZnO/CNT

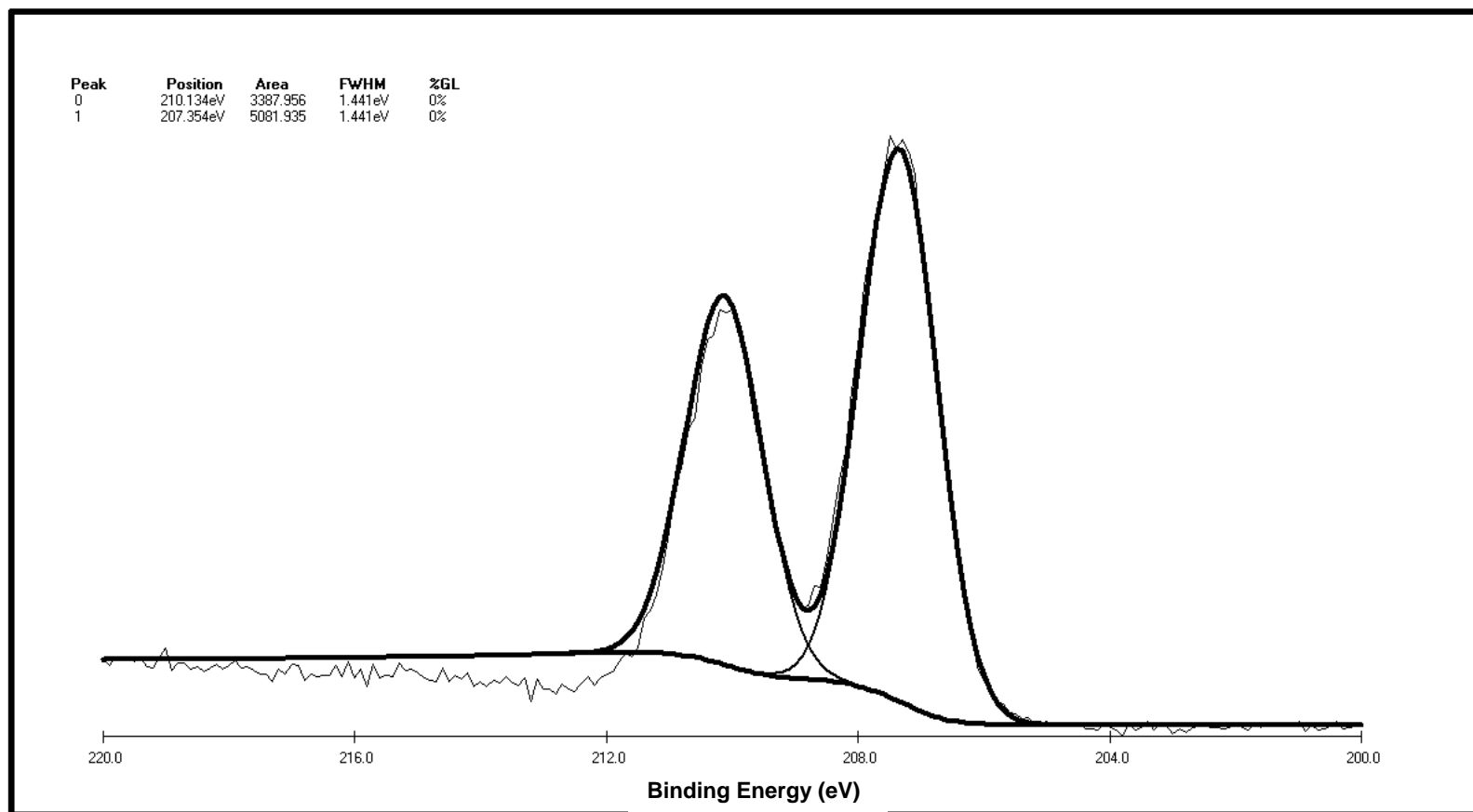


Fig. S-3. Binding energy of Nb<sub>3d</sub> of Nb<sub>2</sub>O<sub>5</sub>/CNT

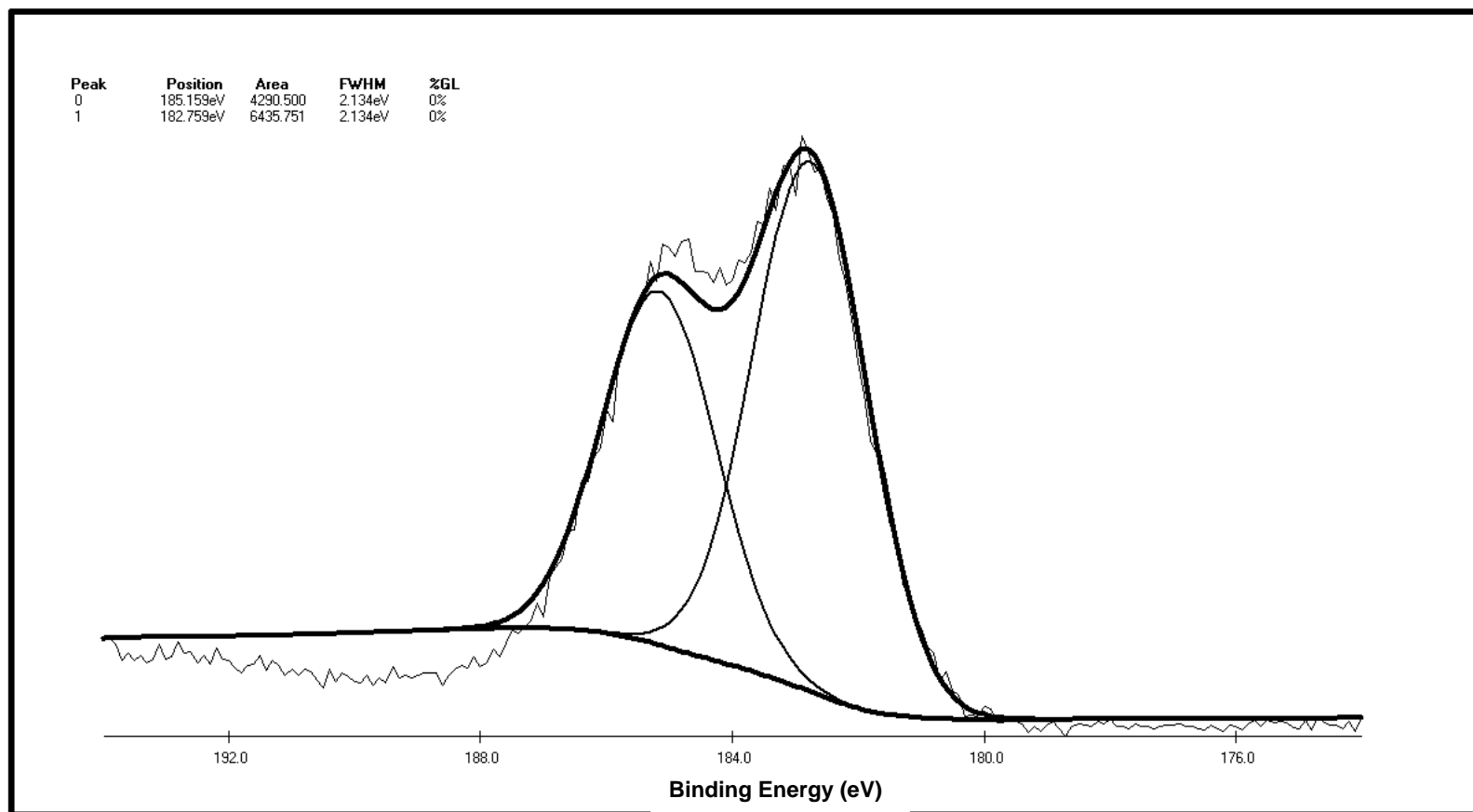


Fig. S-4. Binding energy of Zr<sub>3d</sub> of ZrO<sub>2</sub>/CNT

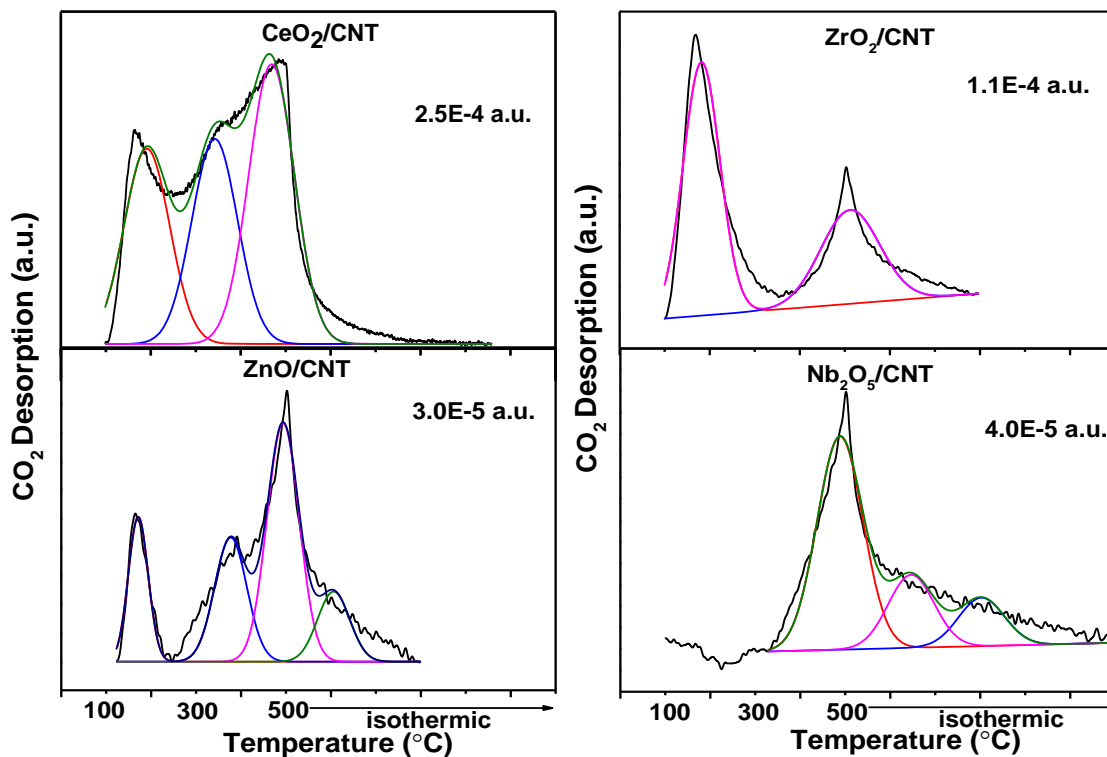


Fig. S-5. CO<sub>2</sub>-TPD of different catalysts

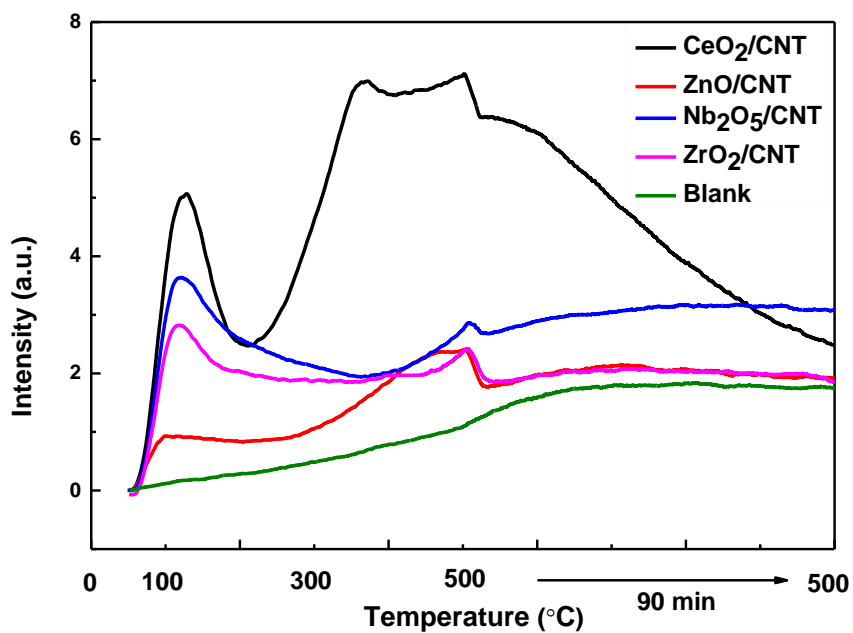


Fig. S-6. NH<sub>3</sub>-TPD of different catalysts

### Peak Analysis

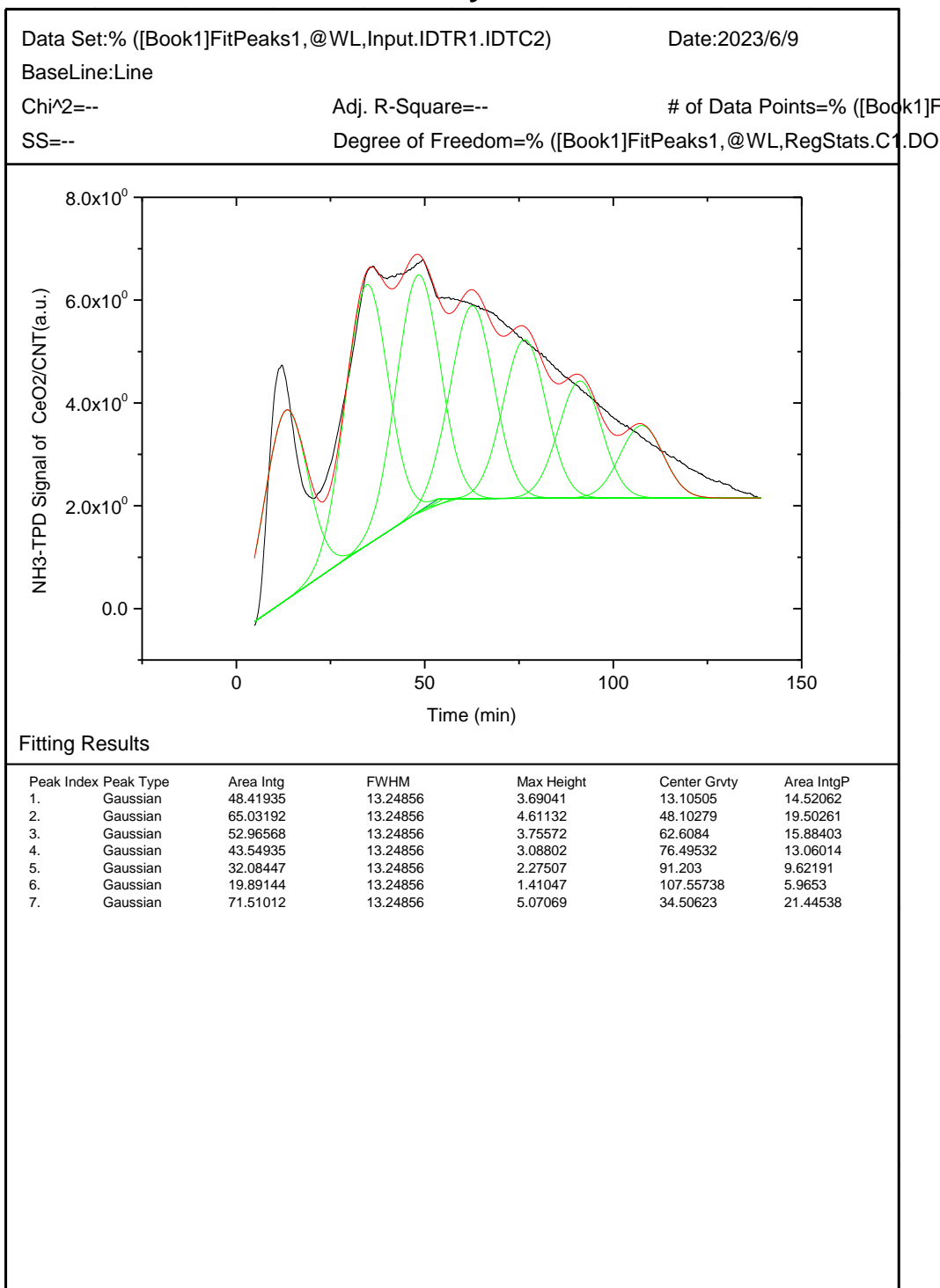


Fig. S-6-1. NH<sub>3</sub>-TPD of CeO<sub>2</sub>/CNT

### Peak Analysis

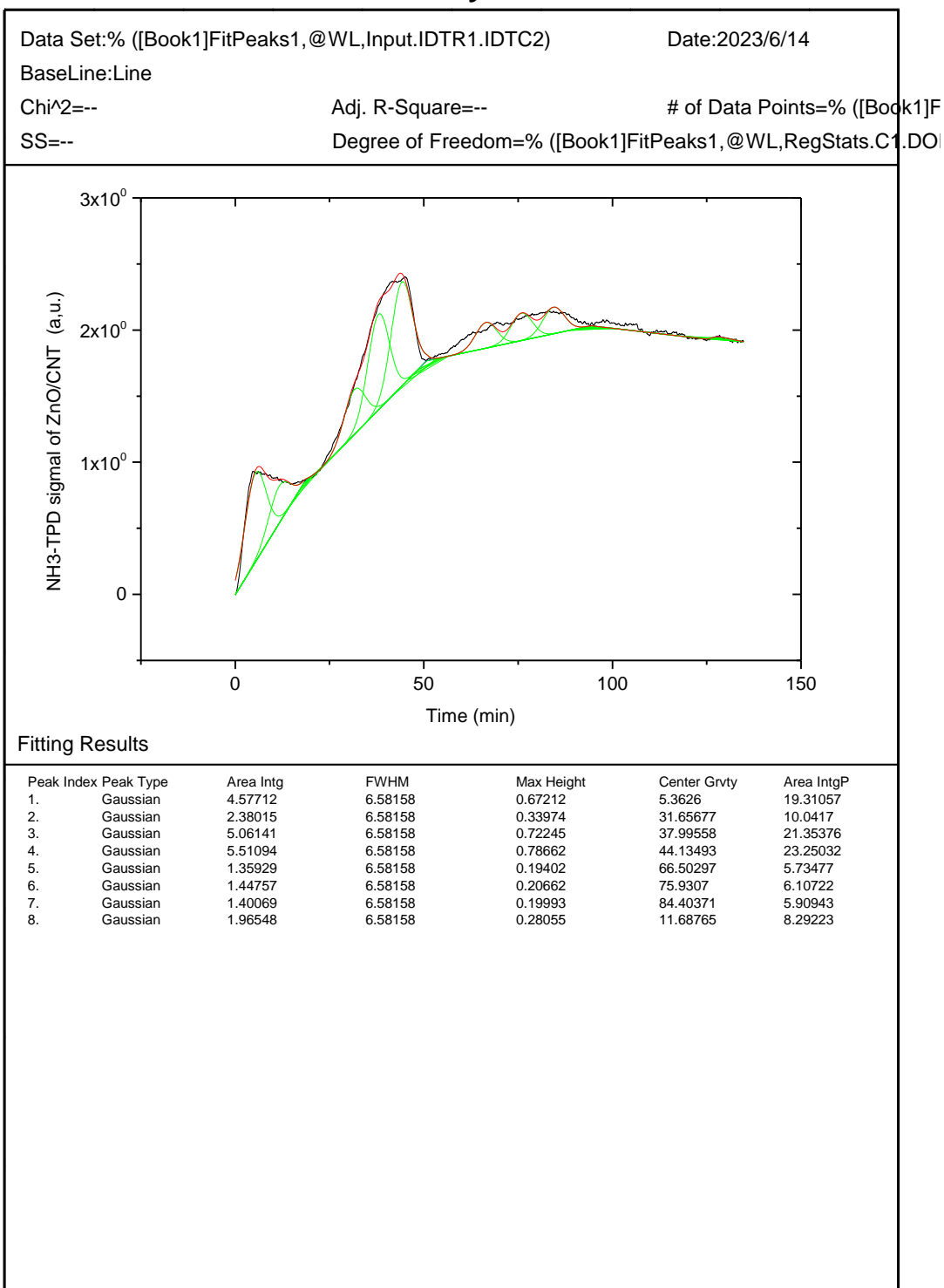


Fig. S-6-2. NH<sub>3</sub>-TPD of ZnO/CNT

### Peak Analysis

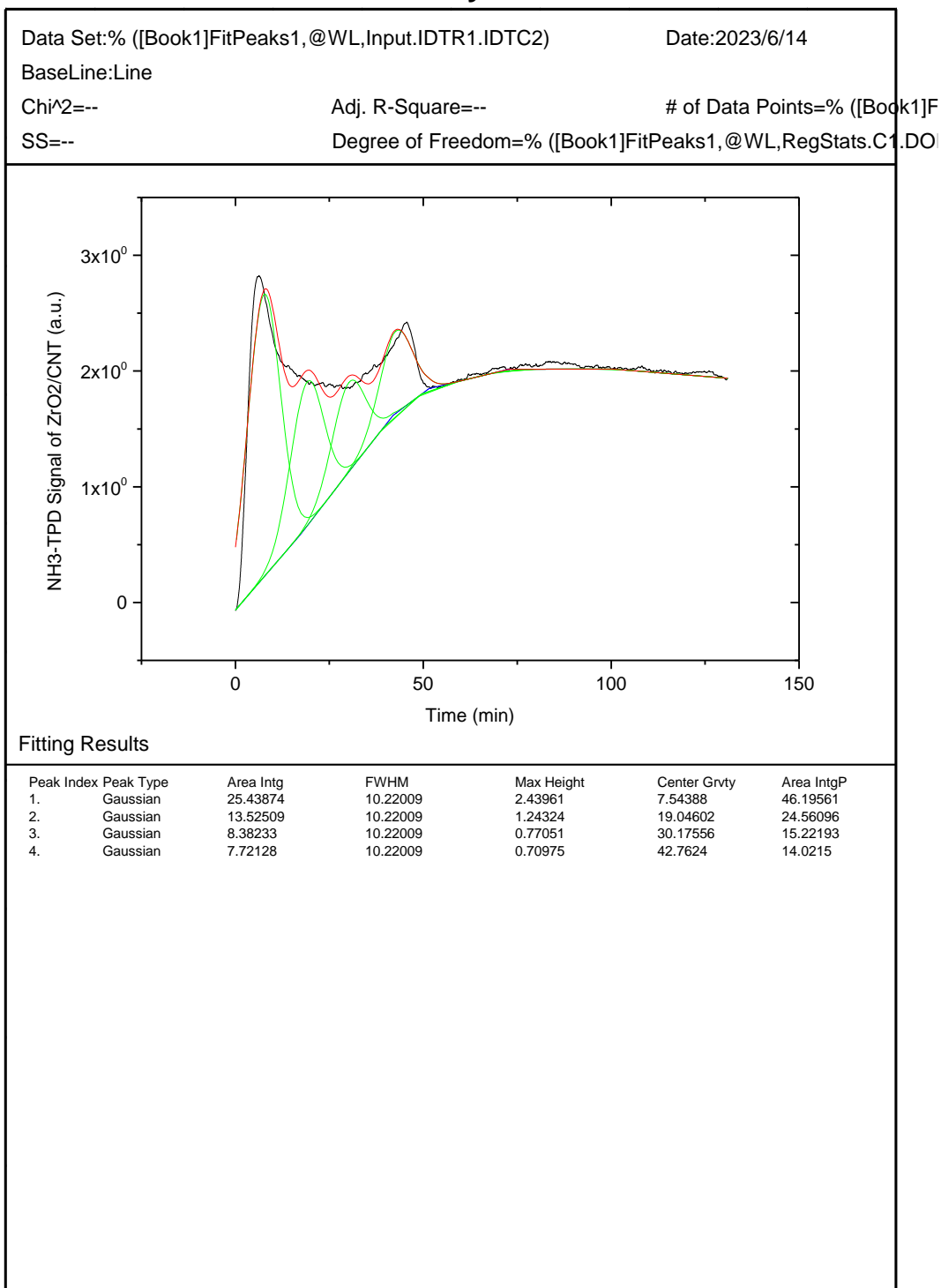


Fig. S-6-3. NH<sub>3</sub>-TPD of ZrO<sub>2</sub>/CNT

### Peak Analysis

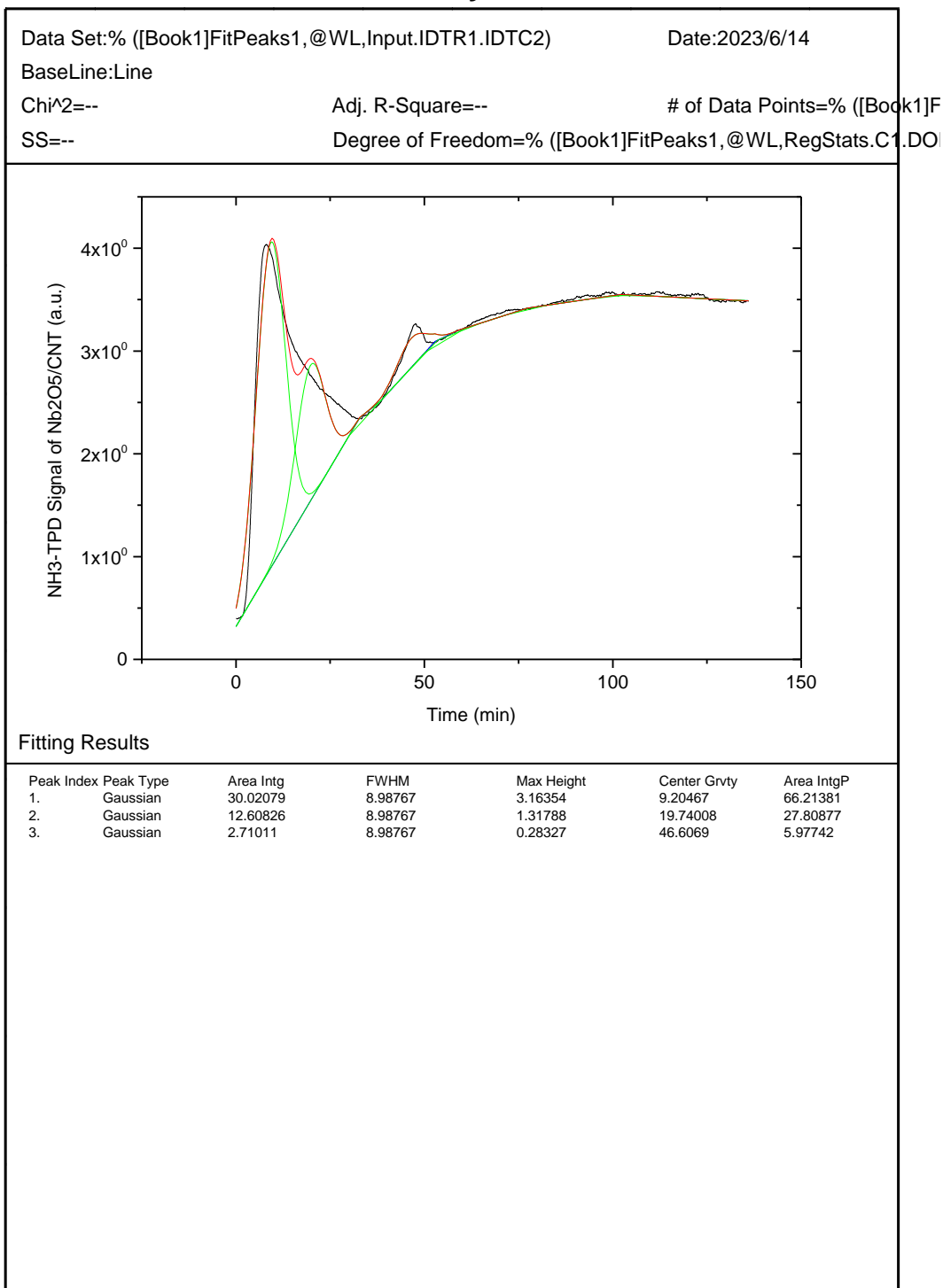


Fig. S-6-4. NH<sub>3</sub>-TPD of Nb<sub>2</sub>O<sub>5</sub>/CNT